

电弧喷涂镍基涂层腐蚀及磨损行为

赵晓舟¹, 周正¹, 贺定勇¹, 赵秋颖², 李冉¹, 蒋建敏¹

(1. 北京工业大学材料科学与工程学院, 北京 100124; 2. 北京工业大学机械工程博士后流动站, 北京 100124)

摘 要: 针对 WTE 垃圾焚烧炉过热器热腐蚀及磨损问题, 设计开发了新型镍基粉芯丝材, 并采用电弧喷涂方法在 SA213-T2 基体表面制备相应涂层. 利用 XRD, SEM, 磨粒磨损试验机及高温箱式电阻炉等对涂层组织结构、磨损及热腐蚀行为进行研究. 结果表明, 所制备涂层具有热喷涂典型的层状结构, 组织较为均匀致密, 孔隙率在 3% 左右, 氧化物含量较低. 涂层平均显微硬度约为 351.27 MPa, 相对耐磨性达基体 7 倍以上. 涂层在 800 °C 下的热腐蚀动力学曲线呈典型抛物线形式, 表面生成 NiCr_2O_4 及 Cr_2O_3 氧化膜, 能够有效阻止腐蚀介质向涂层内部的渗透, 使其抗热腐蚀性能远优于基体材料.

关键词: 镍基涂层; 电弧喷涂; 微结构; 热腐蚀; 磨损

中图分类号: TG174.4 **文献标识码:** A **文章编号:** 0253-360X(2013)04-0048-05



赵晓舟

0 序 言

垃圾焚烧发电(waste-to-energy, WTE)技术能够实现垃圾无害化、资源化和减量化等, 是未来应对城市固体废弃物问题的主要发展趋势. 目前 WTE 成套系统实施技术逐步完善, 并已在世界范围内得到推广应用. 然而焚烧炉中关键部件(如过热器)在苛刻服役环境中的热腐蚀和磨损问题一直是限制其可靠运行的主要因素之一^[1]. 近年来, 为减少燃烧过程中 CO_2 及二噁英等有害物质的排放, 提高热能利用率, WTE 正在向更高燃烧室温度方向发展, 也因此对管壁材料的耐蚀抗磨性能提出了更高的要求.

通过热喷涂技术制备表面高温防护涂层以提高过热器管壁材料的服役稳定性被证明是较为有效的方法之一, 而开发新材料并选用适宜的喷涂技术已成为该领域的热点问题. 目前, 国内外针对这方面的研究主要集中在采用超音速火焰喷涂^[2,3]或爆炸喷涂^[4]制备 $\text{Ni}_{80}\text{Cr}_{20}$, NiCrMo , NiCrAlY 及 $\text{Cr}_3\text{C}_2\text{-NiCr}$ 等涂层. 相关结果表明涂层能够显著提高基材在类似环境中的服役寿命. 但这些技术普遍存在工艺设备复杂、粉末利用率较低、后期维护困难以及成本高昂等问题, 难以在实际工程中得到推广应用. 相比之下, 电弧喷涂则在这些方面体现出独特的技术优势, 但现有喷涂丝材及相应涂层的性能难以满足工

况要求, 针对性的研究也极为有限. 基于此, 文中设计开发了新型镍基粉芯丝材, 采用电弧喷涂在 SA213-T2 钢材上制备相应涂层, 并对涂层微观组织结构、高温腐蚀行为及磨损行为进行研究, 探索该技术及材料在 WTE 或类似环境中的应用前景.

1 试验方法

设计开发了直径为 2.0 mm 的新型镍基粉芯丝材, 名义成分(原子分数, %)为: Cr(20~26), B(12~16), C, Si, Mn(2~5), Ni 余量. 基材选用过热器常用的 SA213-T2 钢, 试样尺寸为 20 mm × 15 mm × 5 mm 和 57 mm × 23 mm × 5 mm. 喷涂前对其表面进行除锈、除油等净化处理, 并采用棕刚玉喷砂处理. 采用 TLAS-400C 型高性能超音速电弧喷涂系统制备涂层, 电弧电压 30~32 V, 工作电流 180~220 A, 压缩空气压力 0.6~0.8 MPa, 喷涂距离 200 mm.

利用 SHIMADZU XRD-7000 型多晶 X 射线衍射仪(XRD)对喷涂态及腐蚀后涂层表面的相结构进行分析. 涂层微结构通过 HITACHI-S 3400N 扫描电子显微镜(SEM)进行表征. 结合 Image Pro Plus 图像分析软件测定涂层孔隙率, 随机选取 15 个区域并计算其平均值. 热腐蚀试验在箱式电阻炉内进行, 结合实际工况选取(Na_2SO_4 -10% NaCl , 原子分数)混合盐溶液作为腐蚀介质^[5,6], 将混合盐溶液均匀涂敷于试样表面并在 120 °C 下烘干, 涂盐量控制在 3~5 mg/cm^2 , 试验温度 800 °C. 腐蚀周期共 200 h,

收稿日期: 2012-02-27

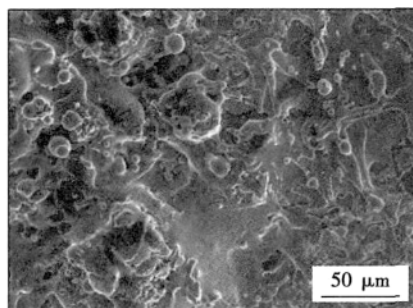
基金项目: 北京市属市管高等学校人才强教计划资助项目(009000-543111505)

每 10 h 取出试样空冷,并用 BS224S 型分析天平(精度 0.1 mg)称重.采用 MLS-225 型湿砂橡胶轮式磨粒磨损试验机测试涂层磨损性能,试验条件为橡胶轮转速 240 r/min,载荷 100 N,磨料选取 40~70 目石英砂,经 1 000 转预磨、2 000 转精磨后,超声波清洗、烘干、称重,计算其较基体的相对耐磨性.

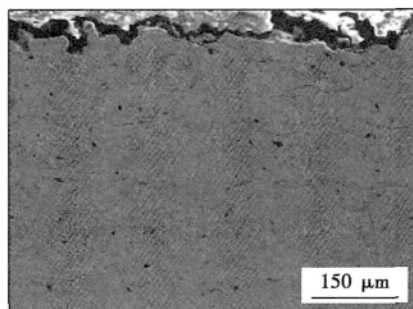
2 结果与分析

2.1 涂层组织结构

图 1 为喷涂态镍基涂层典型的表面(图 1a)及截面形貌(图 1b).涂层表面可见扁平化粒子铺展良好,在连续喷涂逐层沉积过程中,有利于较为充分地填充搭接结构的空隙,提高涂层致密度.从截面形貌可以看出,涂层具有热喷涂典型的层状结构特征,组织较为均匀致密,涂层内部无粗大孔隙和明显裂纹,氧化物含量也较低,并且与基材结合良好.



(a) 表面形貌



(b) 截面形貌

图 1 镍基涂层喷涂态表面、截面形貌

Fig. 1 Surface and cross-sectional morphologies of as-deposited Ni-based coating

通过图像分析软件测定涂层平均孔隙率约为 3% 左右,在电弧喷涂涂层中处于相对较低的水平.孔隙的形成主要来源于涂层搭接堆积的特征和熔融粒子的体积收缩,以及喷涂时溶解于熔融粒子中的气体冷却至室温后析出等^[7].涂层中较为均匀的组织分布和较高的致密化程度,对其在苛刻腐蚀环境

中的服役表现具有积极的影响.

2.2 涂层热腐蚀行为

图 2 所示为涂层与基材在 800 °C 下经 200 h 涂盐腐蚀后,得到的热腐蚀动力学曲线.可以看出基材腐蚀极为严重,其腐蚀增重量与时间呈近似线性关系;同时,坩埚内有持续增多的剥落氧化皮,表明基体表面发生了氧化膜形成、剥落、再形成的循环过程,这种逐层剥落的特征体现出基材表面生成的氧化物在如此恶劣的环境中无法起到有效的防护作用,从而导致基材较高的腐蚀速率.相比之下,涂层腐蚀曲线呈典型的抛物线形式,并且腐蚀速率远低于基材,经全部腐蚀周期后其增重量仅为基体的 1% 左右.另外,在测试过程中涂层始终保持完整形貌,未出现任何开裂、翘起或剥落现象,表明其能够对基材起到有效的防护作用.

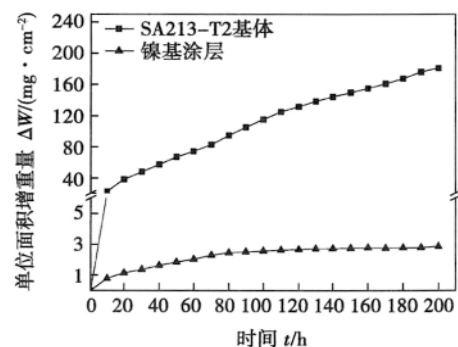


图 2 镍基涂层及 SA213-T2 基体在涂盐介质为 Na_2SO_4 -10%NaCl 腐蚀温度 800 °C 环境下腐蚀动力学曲线

Fig. 2 Thermo-gravimetric curves of coatings and substrate subject to hot corrosion for 200 h in Na_2SO_4 -10 wt. % NaCl environment at 800 °C

图 3 为热腐蚀前后涂层表面相结构对比,可见喷涂态涂层以 NiCr 相为主,并含有一定量的 Ni_3B 相.热腐蚀后,涂层表面生成了大量的氧化物相,并主要为 Cr_2O_3 和 NiCr_2O_4 尖晶石结构.观察热腐蚀测试后涂层的表面形貌可以发现,其较喷涂态试样发生明显改变(图 4).原有平滑的粒子铺展变形形貌完全消失,代之以大量团簇在一起的针状组织所覆盖,并在其间隙位置裸露出部分底部的层片状组织特征.通过 EDS 对两种组织的成分进行分析可知,针状组织主要包含 Ni, Cr, O 三种元素,而层片状组织则以 Cr 和 O 元素为主,仅含有少量 Ni 元素.这与 XRD 分析结果具有较好的一致性.腐蚀后涂层表面的针状组织主要为 NiCr_2O_4 尖晶石结构,而层片状组织则以 Cr_2O_3 相为主.所设计电弧喷涂镍基涂层腐蚀后表面的相结构和形貌特征,与大多数

NiCr 合金及其涂层的热腐蚀结果具有一定的相似性^[3,4] 这表明粉芯丝材的设计方式和电弧喷涂的实现过程对其热腐蚀反应过程影响并不显著。

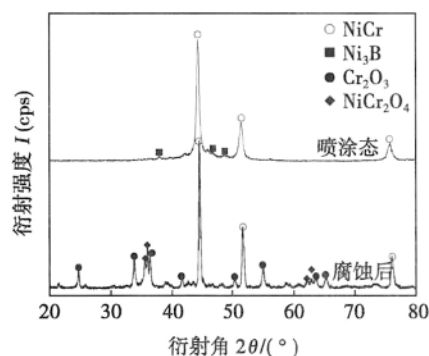


图3 镍基涂层喷涂态及热腐蚀后表面 XRD 图谱

Fig. 3 XRD pattern of as-deposited and corroded Ni-based coatings

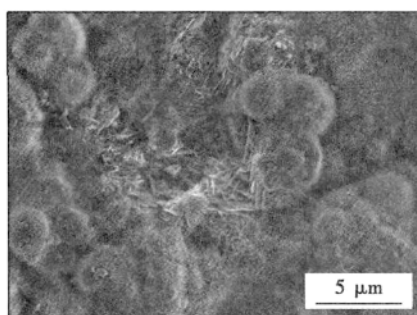


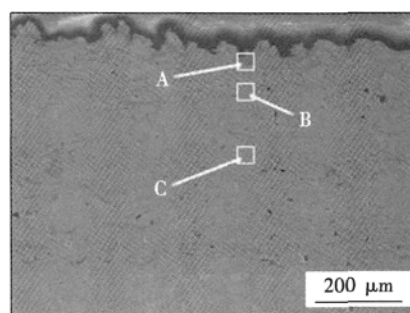
图4 镍基涂层热腐蚀后表面形貌

Fig. 4 Surface morphology of corroded Ni-based coating

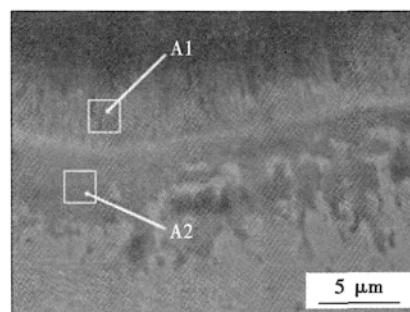
图5 为涂层热腐蚀后截面的典型形貌特征。对比图5a与喷涂态涂层截面图1b得知,在服役周期内所制备涂层保持了较好的完整性,内部无裂纹和厚氧化层的产生,涂层未剥落或减薄,也没有腐蚀介质的贯穿性渗透,有效隔离了腐蚀介质对基体的影响。结合其热腐蚀动力学曲线可以预见,涂层能够在更长服役周期内对基材起到有效的防护作用。

深入观察涂层截面形貌发现,其表层与内部组织存在一定差异。表现在涂层内部到基体与喷涂态组织相比未产生明显变化;而表层则有明显较为连续的灰色氧化相生成,同时在个别变形粒子的弱结合界面处存在一定腐蚀介质渗入所导致的层间氧化产物,但其含量及扩散深度有限且不连续,故在所测试周期内不会对涂层整体服役表现产生显著影响。

从涂层表层典型局部A区的高倍图像中能清晰看到连续的氧化物层形貌(图5b),且氧化物间出



(a) 镍基涂层截面形貌



(b) 局部A区域高倍形貌

图5 镍基涂层热腐蚀后截面形貌

Fig. 5 Cross-sectional morphology of corroded Ni-based coating

现了明显的分层结构。对沿涂层深度方向的几个典型区域进行EDS分析,结果如表1所示。排除B、C等轻元素的影响,最外层A₁区以NiCr₂O₄尖晶石结构为主,连续的A₂区为Cr₂O₃相,代表涂层大部分区域特征的C区与喷涂态涂层组织成分接近,而连接C区与氧化物层的B区则铬含量显著降低,表明其向表层发生了明显的扩散,这主要是由于在抵抗高温腐蚀时铬的氧化物形成的致密膜层是较为有效的。而表面氧化物分层特征的形成主要是由于腐蚀过程中Ni和Cr原子均向涂层表面扩散,并与腐蚀介质接触形成氧化物。虽然Cr原子较Ni原子具有更活泼的化学性质,但因Ni原子扩散速率相对较高,导致涂层表面主要形成NiCr₂O₄尖晶石型氧化物^[8]。该层氧化物的形成有助于降低界面处氧分压,促进次表层连续致密Cr₂O₃膜层的形成^[9]。

表1 热腐蚀前后涂层截面区 EDS 结果(原子分数,%)

Table 1 EDS result of as-deposited and corroded coating

区域	Ni	Cr	O
A ₁	20.65	11.30	68.05
A ₂	5.27	25.97	68.76
B	80.63	19.37	—
C	71.09	28.91	—
喷涂态	70.6	29.4	—

2.3 涂层显微硬度及磨损行为

图6为镍基涂层与SA213-T2基体显微硬度和相对耐磨性的对比结果。喷涂态镍基涂层的平均显微硬度约为 $H_{HV0.1} = 351.27$ MPa, 显著高于常规NiCr涂层^[10], 并达到基材的2.9倍以上。涂层较高的硬度一方面是由于NiCr固溶体的形成, 另一方面来源于大量B元素的引入, 使喷涂过程中形成了部分Ni₃B等硬质相, 对涂层组织起到了有效的强化作用, 能够有效改善其抗塑性变形能力^[11, 12]。硬度值常作为衡量材料耐磨性的重要指标之一^[13], 因此, 涂层较高的硬度也为其带来更为优异的耐磨性能, 使得其相对耐磨性达到基材的7倍以上。

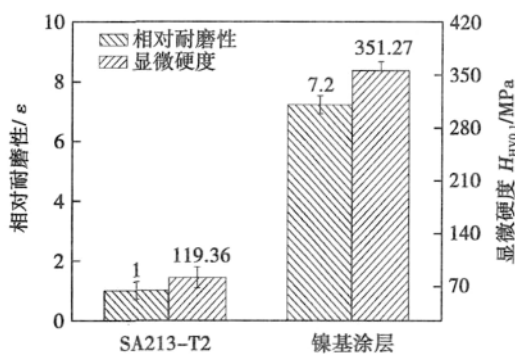
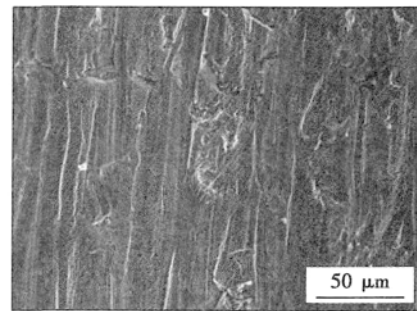


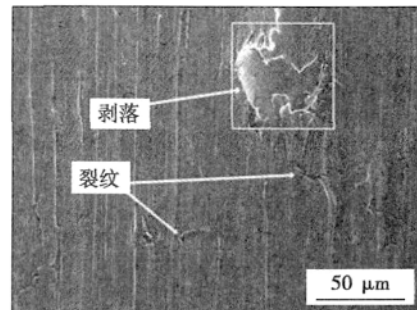
图6 镍基涂层及SA213-T2基体相对耐磨性及显微硬度
Fig. 6 Microhardness and relative wear resistance of Ni-based coating, in comparison with SA213-T2

图7为基体与涂层磨损后典型的表面形貌特征。从图7a可以看出基材表面磨损严重, 沿磨粒运动方向上形成了深浅不等、宽窄不一的连续犁沟, 呈现出典型的塑性切削特征。涂层表面磨损程度较基材有明显改善(图7b), 也存在一定程度的犁削痕迹, 但其深度较浅。这主要是由于涂层较高的硬度, 有效提高了其抵抗塑性变形的能力, 降低了磨粒的切削作用。同时, 在涂层磨损表面还可以观察到明显的裂纹扩展及变形粒子剥落形貌。磨损过程中, 涂层表面局部微区在交变应力作用下造成疲劳损伤, 疲劳损伤累积到一定程度时, 将在变形粒子界面和孔隙等缺陷位置诱发疲劳裂纹。随着裂纹的扩展将导致表层局部微区内聚力降低, 当裂纹达到临界长度时将向涂层表面发生剪切, 造成变形粒子部分或整体剥落。因此, 镍基涂层在磨粒磨损过程中, 其失效形式主要以塑性切削和疲劳磨损为主。

总体来说, 所设计的镍基合金系及相应涂层能够有效改善基材在苛刻服役环境中的腐蚀和磨损性能, 并大幅延长相应构件的使用寿命, 也说明采用粉芯丝材的设计方式和电弧喷涂技术是切实可行的。



(a) SA213-T2基体



(b) 镍基涂层

图7 磨粒磨损后涂层及基体表面形貌

Fig. 7 Surface morphologies of Ni-based coating and SA213-T2 substrate after wearing

3 结 论

(1) 开发了新型镍基粉芯丝材, 并采用电弧喷涂技术制备了相应涂层。涂层具有热喷涂典型的层状结构, 组织较为均匀致密, 孔隙率在3%左右, 氧化物含量较低。

(2) 涂层在800℃下的热腐蚀动力学曲线呈典型的抛物线形式, 其抗腐蚀性能远优于SA213-T2基体材料, 归因于涂层表面生成的NiCr₂O₄及Cr₂O₃氧化膜, 能够有效阻止腐蚀介质向涂层内部及基材的进一步渗透侵蚀。

(3) 涂层平均HV0.1显微硬度约为351.27 MPa, 其相对耐磨性达到基材的7倍以上。涂层磨粒磨损失效形式主要为塑性切削和疲劳磨损。

参考文献:

- [1] Yuuzou K. Application of high temperature corrosion-resistant materials and coatings under severe corrosive environment in waste-to-energy boilers[J]. Journal of Thermal Spray Technology, 2007, 16(2): 202-213.
- [2] Sidhu T S. Oxidation and hot corrosion resistance of HVOF WC-NiCrBSi coating on Ni and Fe based superalloys at 800℃[J]. Journal of Thermal Spray Technology, 2007, 16(5): 844-

- 849.
- [3] Tao K, Zhou X L, Cui H, *et al.* Oxidation and hot corrosion behaviors of HVAF-sprayed conventional and nanostructured NiCrC coatings[J]. Transactions of Nonferrous Metals Society of China, 2007, 19(5): 1151-1160.
- [4] Subhash K, Jayaganthan R, Satya P. Evaluation of cyclic hot corrosion behavior of detonation gun sprayed Cr₃C₂-25% NiCr coatings on nickel-and iron-based superalloys [J]. Surface & Coatings Technology, 2009, 203(8): 1004-1013.
- [5] Gurrappa I. Hot Corrosion Behavior of CM 247 LC alloy in Na₂SO₄ and NaCl environment[J]. Oxidation of Metals, 1991, 51(2): 353-382.
- [6] Yuuzou K. High temperature corrosion mechanisms and effect of alloying elements for materials used in waste incineration environment[J]. Corrosion Science, 2002, 44(2): 223-245.
- [7] Sobolev V V, Guilemany J M. Investigation of coating porosity formation during High-Velocity Oxy-Fuel (HVOF) spraying [J], Materials Letters, 1994, 18(5/6): 304-308.
- [8] Calvarin G, Molins R, Huntz A M. Oxidation mechanism of Ni-20Cr foils and its relation to the oxide-scale microstructure[J]. Oxidation of Metals, 2000, 53(1/2): 25-48.
- [9] Otero E, Pardo A, Perosanz F J, *et al.* Surface modification of several steels after their exposure at high temperature to oxygen and sulfur mixtures[J]. Surface & Coatings Technology, 1995, 76(1/3): 53-60.
- [10] Bala N, Singh H, Prakash S. Accelerated hot corrosion studies of cold spray Ni-50Cr coating on boiler steels [J]. Materials and Design, 2010, 31(1): 244-253.
- [11] 王从曾. 材料性能学[M]. 北京: 北京工业大学出版社, 2001.
- [12] Krishnaveni K, Narayanan T S N S, Seshadri S K. Electroless Ni-B coatings: preparation and evaluation of hardness and wear resistance[J]. Surface & Coating Technology. 2005, 190(1): 115-121.
- [13] 何肇基. 金属的力学性质[M]. 北京: 冶金工业出版社, 1989.

作者简介: 赵晓舟,男,1986年出生,硕士研究生. 主要从材料表面工程技术研究. Email: 603011866@qq.com

通讯作者: 周正,男,博士. Email: zhouzhengbjut@bjut.edu.cn

[上接第37页]

但随着需要识别姿态的特征维数增加,最速下降法识别焊枪姿态的识别率逐渐降低. 实验表明对于焊枪姿态的识别,可通过减少特征维度来提高识别率,但此时的姿态识别效果会受到一定程度的影响,实际应用中要根据试验情况对比删除不需要识别的特征维数,以提高识别率,加速识别响应.

4 结 论

(1) 提出了一种新型的电弧传感器—摆动旋转电弧传感器,建立摆动旋转弧长数学模型并推导出焊枪空间姿态与弧长变化之间的数学关系.

(2) 采用 Gabor 滤波器不仅消除了焊接中由于短路过渡以及电弧飞溅造成的噪声干扰,而且对特征提取时间减少,特征维数降低,计算量和内存需求减少.

(3) 在焊枪姿态识别中,PCA 的降维处理,可以大幅降低特征维数,从而使计算量大幅降低. 试验结果表明 PCA 的特征值提取,对提高焊枪的姿态识别率具有重要意义.

(4) 通过求解欧氏距离和焊枪姿态模型参数的识别计算而获得当前焊枪姿态的类别以及各姿态量,实验表明需要识别的焊枪位姿量越少,识别的效率越高,识别的响应越快.

参考文献:

- [1] 李志刚,张华,高延峰. 旋转电弧传感器特征谐波法的改进[J]. 焊接学报,2009,30(5): 54-56.
Li Zhigang, Zhang Hua, Gao Yanfeng. Improvement of characteristic harmonic method in rotational arc sensor[J]. Transactions of the China Welding Institution, 2009, 30(5): 54-56.
- [2] Murayama V L, Rao V S. Mathematical modeling of simple seam tracking process applicable in multi-function control robotic welding system[J]. Journal of the Institution of Engineers (India), 2004, 85(9): 20-26.
- [3] 叶建雄. 旋转电弧传感器焊枪倾角检测及水下焊缝跟踪技术研究[D]. 南昌: 南昌大学, 2007.
- [4] 潘际奎. 现代弧焊控制[M]. 北京: 机械工业出版社, 2000.
- [5] 冯白海,刘嘉,殷树言,等. 新型低飞溅高能量短路过渡波形控制技术[J]. 焊接学报, 2009, 27(8): 45-48.
Feng Yuehai, Liu Jia, Yan Shuyan, *et al.* The new type of low spatter and high energy waveform control technology for short-circuiting welding [J]. Transactions of the China Welding Institution, 2009, 27(8): 45-48.
- [6] 杜健辉,石永华,王国荣,等. 基于 PCA Nu-SVR 的水下焊缝偏差识别方法[J]. 焊接学报, 2011, 27(3): 21-24.
Du Jianhui, Shi Yonghua, Wang Guorong, *et al.* Seam offset identification of underwater arc welding using PCA Nu-SVR [J]. Transactions of the China Welding Institution, 2011, 27(3): 21-24.

作者简介: 李湘文,男,1982年出生,博士,讲师. 主要从事焊接设备及自动化等方面的科研和教学工作. 发表论文3篇. Email: hongbo@xtu.edu.cn.

of welding torch and the change of arc length was deduced , and a mathematical model was established for the arc length. Considering the characteristics and complexity of welding arc signal , the Gabor wavelet filter was used to eliminate the noise interference , and the feature vector was extracted from the sample data after filtering , and the dimension of data was reduced. The classifier of welding torch attitude according to the principle of Euclidean distance , real-time identification of the spatial attitude of welding torch was conducted with the steepest descent method of model parameters. The results show that the algorithm for recognition of spatial attitude of welding torch with swing of rotating arc sensor was simple and provided theoretical basis for improving the precision of welding seam tracking.

Key words: spatial attitude; welding torch; rotating arc; arc sensor; welding seam tracking

Low temperature sintering-bonding through in-situ formation of Ag nanoparticles using micro-scaled Ag₂O composite paste

MU Fengwen¹ , ZOU Guisheng¹ , ZHAO Zhenyu¹ , WU Aiping¹ , YAN Jiuchun² , Y. Norman Zhou^{1,3} (1. Key Laboratory for Advanced Materials Processing Technology (Ministry of Education) , Department of Mechanical Engineering , Tsinghua University , Beijing 100084 , China; 2. State Key Laboratory of Advanced Welding & Joining , Harbin Institute of Technology , Harbin 150001 , China; 3. Department of Mechanical and Mechatronics Engineering , University of Waterloo , Waterloo N2L 3G1 , Canada) . pp 38 - 42

Abstract: In order to reduce the cost of using Ag nanoparticle paste as bonding materials in electronic packaging , micro-scaled Ag₂O powders were mixed with triethylene glycol (TEG) to form a paste to replace the Ag particle paste. The reaction mechanism of in-situ formation of Ag nanoparticles , the sintering characteristics of micro-Ag₂O paste at low temperature , and the bonding of Ag-coated Cu bulks using this paste were investigated. The results reveal that the Ag₂O particles in the paste were more easily transformed into Ag nanoparticles than micro-Ag₂O itself , and with increasing the sintering temperature , more Ag nanoparticles formed and grew larger by sintering , accompanied with some gaseous products which could escape easily. The effect of sintering-bonding time on the strength of joints fabricated at 250 °C under a pressure of 2 MPa was analyzed. The average shear strength of the joints increased with sintering-bonding time and reached about 24 MPa when the sintering-bonding time was 5 min. And the microstructure of the fractured surface and the cross-section of typical joints made at 250 °C under 2 MPa were also examined.

Key words: silver oxide; in-situ formation; Ag nanoparticles; sintering bonding

Diagnosis of welding arc ionization region and boundary

XIAO Tianjiao , SONG Yonglun , LI Chao , YAN Sibao (School of Mechanical Engineering and Applied Electronics Technology , Beijing University of Technology , Beijing 100123 , China) . pp 43 - 47

Abstract: Welding arc , as a heat source , converts electric energy to heat energy by gas discharging , and the scale of the arc ionization region as well as the effective range of the arc determines the distribution of its energy density. In this paper , the quantitative detection of argon atoms and argon-ion line intensity were achieved by emission spectroscopy diagnostic method , and the arc ionization region and the gas atom excitation radiation boundary scale were obtained. The measurement not only overcame the problem that the arc could not be quantitatively tested with camera due to exposure factors , but also could be used for observation of pulsed arc. The results provide the basis for better understanding arc physics and modeling the arc.

Key words: tungsten inert gas welding; arc boundary; ionization region; arc geometric pattern; spectroscopy diagnostic

Corrosion and wear behavior of wire-arc sprayed Ni-based coatings

ZHAO Xiaozhou¹ , ZHOU Zheng¹ , HE Dingyong¹ , ZHAO Qiuying² , LI Ran¹ , JIANG Jianmin¹ (1. College of Materials Science and Engineering , Beijing University of Technology , Beijing 100124 , China; 2. Postdoctoral Research Station of Mechanical Engineering , Beijing University of Technology , Beijing 100124 , China) . pp 48 - 52

Abstract: A new Ni-based cored wire was designed to prepare coatings by wire-arc spraying on SA 213-T2 substrate in order to solve the corrosion and wear problems in waste-to-energy (WTE) plants. According to X-ray diffractometry (XRD) and scanning electron microscopy (SEM) analysis , the as-deposited coatings with low content of oxide phases presented uniform and dense layered structure with porosity at around 3% . The wear resistance of the designed coating , about 7 times higher than that of the substrate , was measured by a rubber wheel abrasive testing machine. Thermo-gravimetric technique was used to investigate the high-temperature corrosion behavior of the coatings in molten salt environment (Na₂SO₄ - 10% NaCl) at 800 °C in a muffle furnace. As a result , the weight gain curve of the coating followed the parabolic law and presented extremely lower corrosion rates , comparing with that of the substrate , due to the formation of Cr₂O₃ and NiCr₂O₄ oxide films on the surface which prevented the diffusion or penetrating of corrosive species. Consequently , the developed coating could provide much better corrosion resistance properties than SA213-T2 substrate.

Key words: Ni-based coating; arc spraying; microstructure; hot corrosion; wear behavior

Recognition of weld flaw based on feature fusion of ultrasonic signal and image

HU Wengang , GANG Tie (State Key Laboratory of Advanced Welding and Joining , Harbin Institute of Technology , Harbin 150001 , China) . pp 53 - 56

Abstract: Ultrasonic testing is widely applied to detect the inner flaws of materials , but it is still difficult to recognize the flaw properties. In this paper , a new method for flaw recognition based on feature fusion of ultrasonic signal and image was proposed. The detection data was used to identify the weld flaw by the data fusion of ultrasonic signal feature and morphological feature. The welds containing defects such as hole , slag , crack ,